Studying the Structural Dynamics of Bipedal DNA Motors with Single-Molecule Fluorescence Spectroscopy

Rula Masoud, Roman Tsukanov, Toma E. Tomov, Noa Plavner, Miran Liber, and Eyal Nir*

Department of Chemistry and the Ilse Katz Institute for Nanoscale Science and Technology, Ben-Gurion University of the Negev, Beer-Sheva, Israel

ABSTRACT

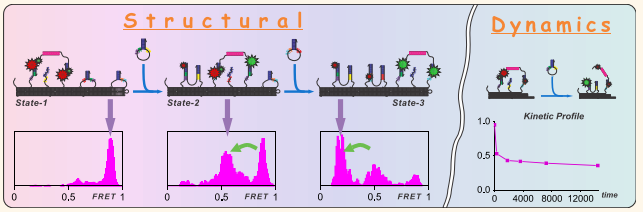

We present a test case example of a detailed single-molecule fluorescence study of one of the most sophisticated and complex DNA devices introduced to date, a recently published autonomous bipedal DNA motor. We used the diffusion-based single-molecule Förster resonance energy transfer technique, coupled to alternating laser excitation (sm-FRET—ALEX), to monitor the motor assembly and operation. The study included verification of the formation of the correct structures, and of the correct motor operation, determination of the formation and stepping reaction yields, and identification of side products. Finally, the mechanisms of the motor assembly and operation were elucidated by measuring the reaction kinetics profile of track-walker binding and of lifting of the walker's leg upon fuel addition. The profiles revealed a fast phase, in which about half of the reaction was completed, followed by a slow phase which adds somewhat to the yield, reflecting the incomplete motor assembly and operation identified in the equilibrium experiments. Although further study is needed to fully understand the reasons for the incomplete assembly and operation, this work demonstrates that single-molecule fluorescence, based on its ability to provide detailed *in situ* structural dynamics information, inaccessible for traditional methods, constitutes an excellent tool for chaperoning the development of DNA-based technology.

KEYWORDS: single-molecule fluorescence · FRET · ALEX · DNA motor · DNA nanotechnology · DNA dynamics

Achieving a high degree of control over the physical world is one of the major endeavors of modern science and technology. A promising path toward realization of this goal at the molecular level rests on DNA-based technology, as is evident from the numerous recently demonstrated structures,[1] motors,[2,3] robots,[4] computers,[5] molecular assembly line,[6] and carriers to deliver drugs,[7] made from DNA. As is the case for all technological design processes—whether for macro- or microdevices—development relies on high-quality, reliable feedback on the properties of the both building blocks and the final products; for molecular devices, these properties include structure, dynamics, and interactions. However, acquiring such feedback at the molecular level remains a challenging task. Even though most of the effort in the development of a molecular device is often devoted to molecular analysis, the information acquired may be limited in both quality and scope, thereby hindering progress.

In the DNA nanotechnology field, building blocks and final products are typically studied using gel, bulk fluorescence, atomic force microscopy (AFM), and transmission electron microscopy (TEM) techniques, each with its particular advantages and disadvantages. Since gel, TEM, and ambient AFM are not *in situ* techniques, in that samples have to be transferred from a favorable aqueous environment to a possibly harmful environment, they have two major inherent disadvantages. First, it is difficult or even impossible to measure time-dependent conformational changes, which are of particular interest in the development of dynamic devices. Second, there is a risk of damage to the samples such that the acquired data may not accurately reflect the subject or the state of interest. In answer to these problems, some progress has recently been made with the use of solution AFM to monitor *in situ* the progress of motors along a DNA-origami track,[8,9] but the method still has inherent drawbacks in that temporal and spatial resolution are limited, data acquisition is a tedious process, and the technique is not suitable for a system lacking a solid platform, such as origami, as studied here. Fluorescence methods, whether bulk or single-molecule, are undoubtedly the methods of choice for studying structural dynamics. Indeed, bulk fluorescence was extensively used;[5,9−11] however, when applied

* Address correspondence to Eyalnir@bgu.ac.il.

Received for review April 18, 2012 and accepted June 4, 2012.

Published online June 04, 2012
10.1021/nn301709n

to a complex system, it often failed to capture the real complexity of the sample, since different populations within the sample may contribute to the detected signal, possibly resulting in erroneous interpretation of the data. Moreover, while in single-molecule experiments kinetic measurements can be performed in equilibrium conditions, for example when the sample is immobilized, in bulk, kinetic measurements require nonequilibrium conditions, which are not always easy to achieve.

The single-molecule fluorescence approach has become a major tool for unraveling structural dynamics and interactions of DNA,[12] RNA,[13] proteins,[14] and DNA–protein complexes,[15,16] but in the DNA nanotechnology field, the method is still not widely applied.[17–20] The approach, which comprises a number of different methods,[21] offers a unique combination of features that enables molecular analysis beyond what is possible with methods regularly used, thereby expanding the tool-kit available for developing a DNA-based nanotechnology. The method described here, single-molecule Förster resonance energy transfer, coupled to alternating laser excitation (sm-FRET–ALEX),[22–25] embodies many of the advantageous features of the approach. The noninvasive nature of the fluorescence method allows *in situ* measurements to be performed while the system is maintained in an aqueous environment. With the FRET technique, structural dynamics can be studied with high spatial and temporal resolution, and with the implementation of multiple excitation lasers (ALEX) species stoichiometry can be determined enabling the sorting of subpopulations.

To address the problem of coordinated motion between motor legs, Omabegho *et al.*[26] recently constructed one of the most sophisticated and complex DNA motors introduced to date, an autonomous DNA bipedal walker that coordinates the action of the two legs by cyclically catalyzing the hybridization of metastable DNA fuel strands, a process that results in a chemically ratcheted walk along a directionally polar DNA track. To monitor the motor assembly and progress, they used nondenaturing and superdenaturing polyacrylamide gel electrophoresis (PAGE), radioactively labeled DNA strands, and psoralen-labeled DNA strands, which under exposure to ultraviolet radiation, covalently cross-link to neighboring DNA strands *via* a T base (*i.e.,* stem loop to walker's leg). The nondenaturing gel was used for verifying the formation of the building blocks and of the complete motor. The superdenaturing gel was used to monitor the motor's progress by determining the presence/absence of covalently bound legs and stem loops, which are indicative of the walker's position on the track. It is impotent to remember, however, that with the gel technique, preparation and measurements takes a long time—of the order of hours—which may make it inadequate for dynamic measurements.

Here we show how the diffusion-based sm-FRET-ALEX technique is used to monitor the assembly and operation of dynamical DNA devices. As our model system, we used the autonomous bipedal DNA motor of Omabegho *et al.*[26] We began by verifying the formation of the correct structures and determining the formation yields. Then, to demonstrate the operation of the motor, we measured three motor resting states as the motor progressed upon addition of the DNA fuel strands, determined the yields of the stepping reactions, and identified side products. Finally, continuing beyond the proof of principle of the study of Omabegho *et al.*,[26] we elucidated the mechanisms involved in the assembly and operation phases of the motor by measuring the reaction kinetics profile of track-walker binding and of lifting of the walker's legs upon the addition of the fuel strands.

RESULTS

Principle of the sm-FRET–ALEX Technique. For comprehensive introduction to the technique, see the Supporting Information, Figure S1, the Methods section, and previous publications.[22,24] In short, the FRET efficiency (*E*) of each photon burst (molecular species diffuses thought the confocal spot) is calculated (eq 1 in the Methods) and incorporated into an *E*-histogram that reflects the donor–acceptor distance. Similarly, the donor–acceptor brightness ration (*S*) is calculated (eq 2 in the Methods section) and incorporated into a *S*-histogram that reflects the fluorophore's stoichiometry. Together, the *E* and the *S* generate a two-dimensional spectroscopy that reports on the species' structure and presence or absence of labeled components.

Motor Assembly and Operation Principle. A brief description of the assembly and operational principle of Omabegho *et al.*[26] and of our motors is given in Figure 1. Eighteen DNA strands form a 49-nm double-crossover track which held four metastable stem loop hairpins, and a walker, which unlike Omabegho *et al.*,[26] who used phosphoramidites to covalently bind the walker's two legs, is made of two hybridized ssDNAs. For other differences between our motors and the setup of Omabegho *et al.*,[26] see the Supporting Information.

Monitoring the Assembly of the Motor's Building-Block. For reasons of clarity, we start by presenting the sm-FRET–ALEX results for the assembly of simple building blocks and then proceed to those for building blocks with increased complexity. In reality, it is not always necessary to strictly adhere to a bottom-up approach or to examine the formation of all building blocks. In this study, we generally followed the design, preparation, and operation procedures of Omabegho *et al.*[26] First, we examined the binding reactions of the L-O and L-E walker's legs to the stem loops T1–4 (Figure 2

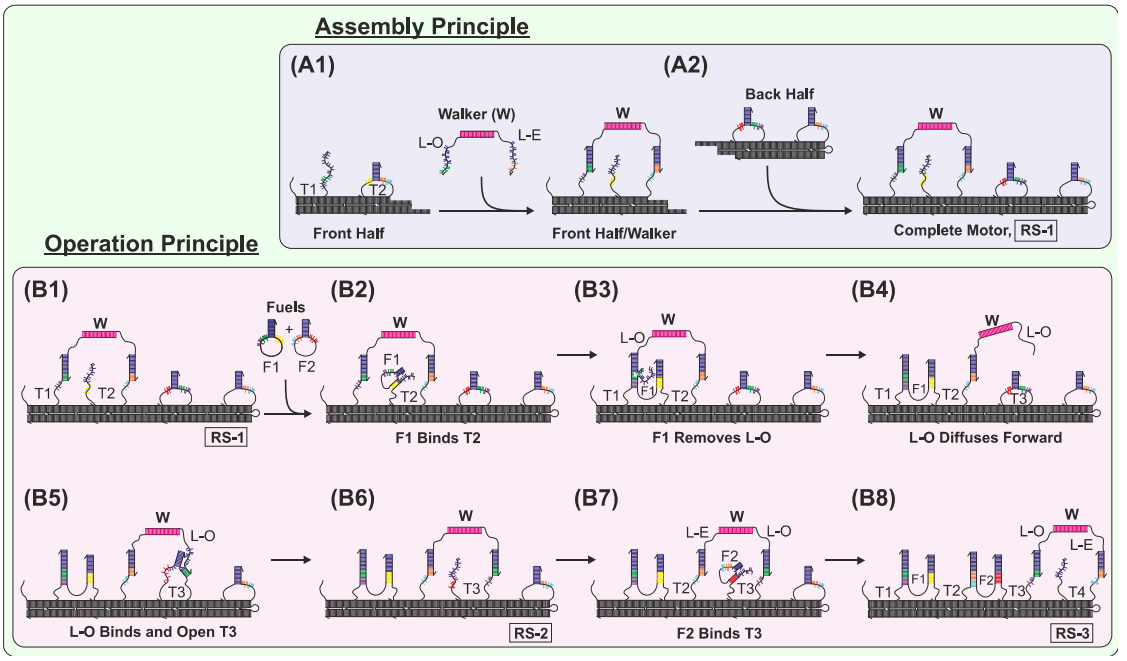

Figure 1. Schematic presentation of the motor's assembly and principle of operation, as designed by Omabegho *et al.*,[26] with our minor modifications. Assembly principle: (A1) The preannealed front half of the track and the preannealed walker are mixed at room temperature (designated cold mixing; see Methods). The walker's legs, designated Leg-Odd (L-O) and Leg-Even (L-E), bind stem loop-1 and stem loop-2 (designated T1 and T2) to form the front half/walker complex. The preannealed back half is added (cold mixing), and, *via* complementary strands, connects to the front half to form the complete motor at Resting State-1 (RS1). Operation Principle: RS-1 is cold mixed with hairpin fuel-1 and fuel-2 (F1 and F2). First, F1 binds to T2 (*via* the free stem of T2) and opens through branch migration (B2). After opening, the free single strand of F1 migrates to T1, attaches itself to a free complementary toehold sequence located on the lower part of T1 (B3), and through branch migration, releases L-O. The free L-O stochastically diffuses forward toward T3 (B4), attaches itself to a short toehold located on T3 (B5), and through branch migration, opens T3, freeing its left stem to complete RS-2 (B6). Now (but not before) F2 is recruited by binding to the newly freed stem (B7), and in a process similar to that present in B2 to B6, free L-E to immigrate forward toward T4 and bind it to complete RS-3 (B8).

A1−5). The reactants were mixed at room temperature, at a concentration of 500 nM, and incubated for 1 h. Aliquots of 1-μL of the mixtures were diluted (separately) to a concentration of 3 pM, and measured using the sm-FRET−ALEX setup. The single-molecule measurement provided the distribution of the *E* and *S* values. The donor-only and the acceptor-only reactants appeared at $S = \sim 0$ and $S = \sim 0.9$, respectively, and the doubly labeled product appeared at $S = \sim 0.5$.

To verify that the products had adopted the correct structure, the averaged *E* value (of the *S*-based selected population, inside the pink dashed rectangle), which reflects the donor−acceptor distance, was compared with the designed distance [mentioned in Figure 2 in the number of base pairs (bp) and with a known scale of dsDNAs of various lengths (data not shown)]. Indeed, all constructs yield the right *E* values. The reaction yield was evaluated by comparing the size of the product population with the sizes of the reactant populations (81%, 80%, 87%, and 93%, for reactions A2, A3, A4, and A5, respectively). The fact that most of the reactants had interacted to form a walker/stem loop complex confirmed that the walker's legs were indeed capable of opening the stem loop hairpins, even at room temperature, as is later required for a functioning motor. The presence of sizable donor-only or acceptor-only populations indicated that reactions were incomplete (Figure 2, A2−5) as will be later discussed.

Using the annealing procedure, conducted with concentrations of 500 nM for 1.5 h, we examined the formation of the walker from its L-O and L-E legs, the binding of the walker to T1, and the assembly of the track's front and back halves (Figure 2,B1−5). To form the complete track, preannealed front and back halves were cold mixed (250 nM, 1.5 h, Figure 2,B5). Here, too, the *E* and *S* indicate the formation of the designed structures, and the yields were 92%, 83%, 92%, 77%, and 79% for the reactions in Figure 2,B1−5, respectively. For constructs containing of two ssDNAs, the peaks in *S* were well centered on the expected value (Figure 2,A2−5 and B1). For structures containing a higher number of ssDNAs, the histograms were wider, possibly indicating the presence of minor populations not having a single donor and a single acceptor (Figure 2,B3−5) or a single donor and two acceptors (Figure 2,B2), as it should (see discussion about side product, later). For discussion about the expected histograms' width see the Supporting Information.

Monitoring the Assembly of the Complete Motor and Identifying Side Products. To complete the motor assembly,

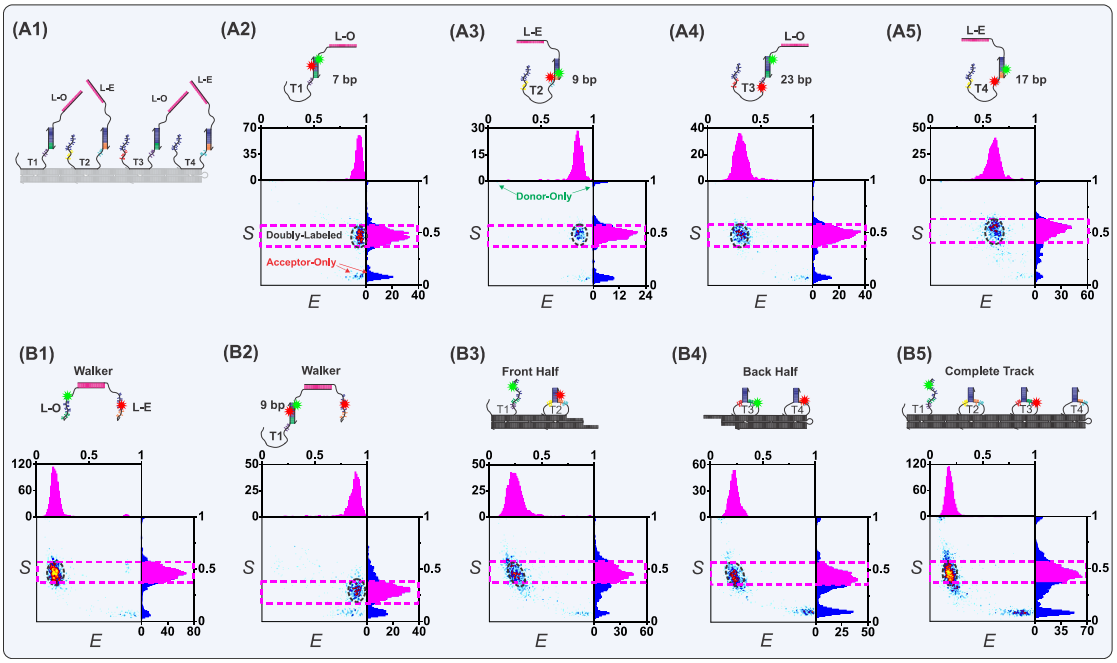

Figure 2. Monitoring the building-blocks assembly by means of sm-FRET−ALEX. For each of the examined mixtures, a two-dimensional *E*/*S* histogram, a one-dimensional *S* histogram and a one-dimensional *E* histogram, and the schematics of the designed product are presented. The donor and acceptor positions (green and red stars, respectively) and the distance between them in number of base-pairs (bp) are given. Except for B2, the *E* histograms were constructed from events with 0.42 < *S* < 0.62 (appears inside the pink dashed rectangles). This range of *S* values indicates the presence of a single donor and a single acceptor. For B2 the *E* histograms were constructed from events with 0.20 < *S* < 0.42, indicating the presence of a single donor and two acceptors. The populations with the expected *S* and *E* values are circled with black dashed lines. Donor-only events appear in the upper-left corners of each *E*/*S* histogram, and acceptor-only events in the bottom-right corners (as indicated in A3 and A2, respectively). (A) Binding of the walker's legs to the stem loops upon cold-mixing. (A1) Schematics of the walker's legs and stem loops in the context of a complete motor. (A2) The walker's Leg-Odd (L-O) labeled with donor and the stem loop-1 (T1) labeled with acceptor form a double helix, which yielded bursts with an average *E* = 0.95, reflecting the short donor−acceptor distance (7 bp). (A3) Similarly, donor-labeled Leg-Even (L-E) and acceptor-labeled stem loop-2 (T2) yielded bursts with *E* = 0.9, as expected from the donor−acceptor distance (9 bp). (A4) Donor-labeled L-O and acceptor-labeled T3 yielded *E* = 0.25, as expected (23 bp). (A5) Donor-labeled L-E and acceptor-labeled T4 yielded *E* = 0.51 (17 bp). (B1−5) Monitoring the interaction between building blocks with increased complexity. (B1) Annealed donor-labeled L-O and acceptor labeled L-E yielded *S* = 0.5 and *E* = 0.15, reflecting the long donor−acceptor distance (∼7 nm). (B2) Annealed donor-labeled L-O, acceptor-labeled L-E, and acceptor-labeled T1 yielded *S* = 0.33, reflecting the presence of one donor and two acceptors, and *E* = 0.9, reflecting the short distance between the donor and the nearby acceptor (9 bp). (B3) Annealed front half with donor-labeled T1 and acceptor-labeled T2 yielded *S* = 0.5 and *E* = 0.15, as expected (donor−acceptor distance, ∼7 nm). (B4) Similarly, annealed back half with donor-labeled T3 and acceptor-labeled T4 yielded *S* = 0.5 and *E* = 0.15, as expected (donor−acceptor distance, ∼7 nm). (B5) Cold mixing of preannealed front (donor-labeled T1) and back halves (acceptor-labeled T3), forming the complete-track with *S* = 0.5 and *E* = 0.15, as expected (donor−acceptor distance ≈14 nm).

according to the procedure of Omabegho *et al.*[26] (as explained in Figure 1A), we separately annealed the front half, the back half, and the walker. First, the front half (labeled with one acceptor on each stem loop) and the walker (labeled with one donor on each leg) were cold mixed and then examined with the single-molecule technique (Figure 3A). The major detected population is the desired front half/walker complex (circled with black dashed line, Figure 3A), however, minor populations were also identified (circled with green and pink dashed lines, Figure 3A). For more about side products see the Discussion section and Figures S2 and S3 in the Supporting Information. The formation yield for the front half/walker complex was 57% (the population inside the black circle). Following the procedure of Omabegho *et al.*,[26] we cold mixed the front half/walker complex with the preannealed back half to form the complete motor at Resting State-1 (RS-1, Figure 4B). The similarity of the results for the front half/walker to those for the RS-1 (the *E*/*S* histograms and the *E* and *S* histograms) indicated that the walker did not begin striding forward upon addition of the back half, as required for normal operation of the motor before the addition of fuel strands (confirmation that the back half binds the front half was given in Figure 2 B5).

Monitoring the Motor Operation. After the assembly of RS-1 had been demonstrated, we studied the motor operation. We measured three resting states, RS-1, RS-2, and RS-3, and evaluated the yields of the stepping reactions (Figure 4A−C, respectively). Experiments demonstrating leg lifting of just the front half/walker complex upon introduction of fuel are shown in Figure S4 in the Supporting Information. We cold mixed a 5-fold excess of fuel-1 with RS-1, incubated the mixture for 1 h and examined using the sm-FRET−ALEX technique. The result clearly shows the appearance of a

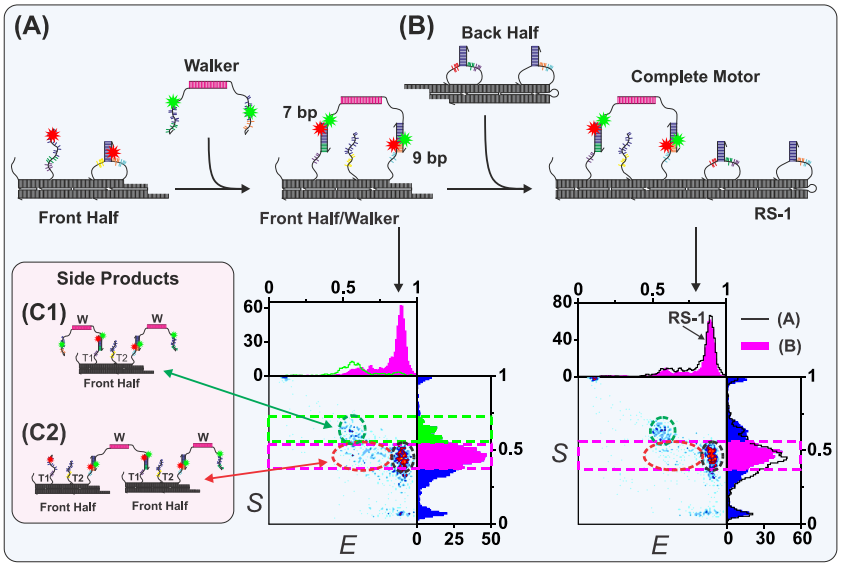

Figure 3. Monitoring the final step of the assembly of the motor and identification of the side products. (A) The preannealed front half and the preannealed walker were cold mixed to form the front half/walker complex. The 2D histogram revealed the expected dominant population (circled with a black dashed line), with $S = \sim 0.5$, reflecting the presence of two donors and two acceptors, and $E = 0.9$, reflecting the close proximity of each of the two donors to an acceptor (7 and 9 bp) and side products (C1 and C2). (B) The front half/walker complex was then cold mixed with the preannealed back half to form the complete motor (RS-1). Two minor side products, one assigned as a single front half bound to two walkers and the other assigned as two front halves bound to two walkers connected *via* T1 and T2 were observed (C1 and C2, and circled with green and red dashed line, respectively). The assignment of the minor populations was based on $0.55 < S < 0.71$ (reflecting the presence of four donors and two acceptors) and $E = 0.55$ (reflecting the close proximity between two donors and two acceptors, while two donors lacked nearby acceptors) and $0.38 < S < 0.55$ (four donors and four acceptors) and $E = 0.5-0.8$ (reflecting the close proximity between three donors and three acceptors while one donor lacked nearby acceptors).

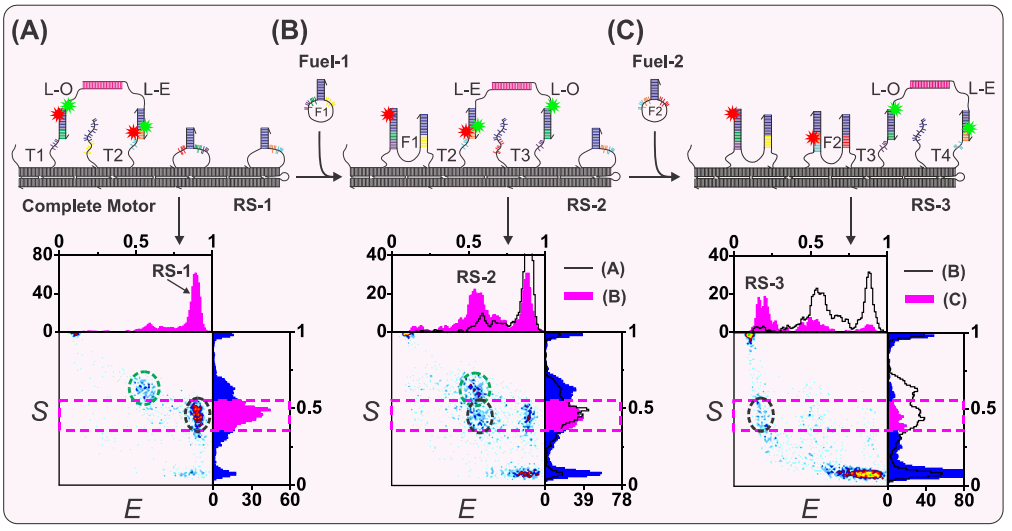

Figure 4. Monitoring the motor activity and the three motor states and estimating the yields of the stepping reactions. (A) The dominant RS-1 ($S = 0.5$ and $E = 0.9$, circled with black dashed line) and the minor side product (circled with green dashed line). (B) Fuel-1 was added to the solution; it bound to T2 (at its free single strand) and removed the L-O from T1, thereby increasing the distance between one of the donors and an acceptor, which was reflected in a decrease in FRET from $E = 0.9$ in RS-1 to $E = 0.55$ in RS-2. The L-O leg then immigrated forward, opened the T3 stem and bound to it to form RS-2 (the L-O T3 binding is not reflected in the results). (C) Fuel-2 was added to the solution; it bound to T3 and removed the L-E leg from T2, thereby increasing the distance between the second donor and an acceptor, which was reflected in an even further decrease in FRET to $E = 0.15$ in RS-3. The increase in acceptor- and donor-only populations reflects the disassembly of the walker from the track.

population with $E = 0.55$ (Figure 4B, circled with black dashed line), as expected for a scenario in which one donor is in close proximity to an acceptor (9 bp) and the other donor is not. The yield of the stepping reaction (63%, calculated as the percentage of RS-1 population that transformed to RS-2) was similar to the yield observed by Omabegho *et al.*[26] (75%), and almost no RS-3 was observed ($E = 0.15$) at this stage, as

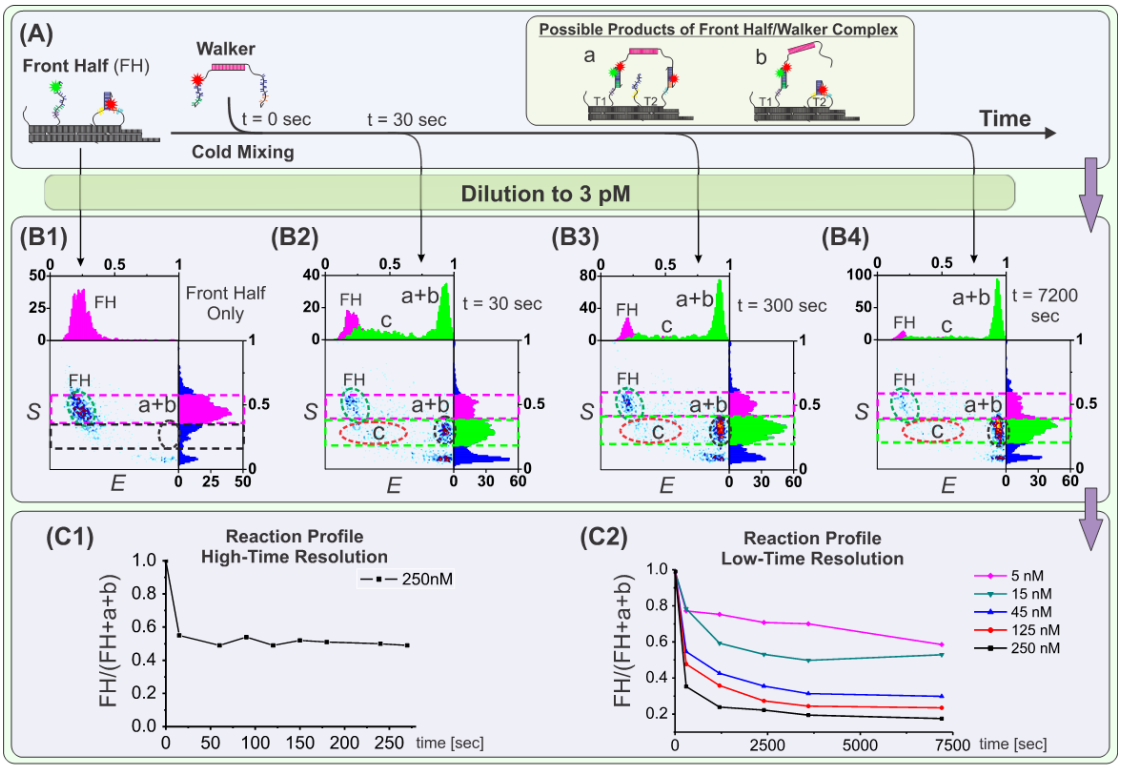

Figure 5. Kinetics of the front half and walker binding reaction. (A) Cold mixing of front half and walker can result inseveral products, for example a, b. (B1−4) The front half (FH) and the walker (250 nM) were cold mixed, incubated for various time periods, and a small fraction of the mixture (1 μL) was diluted to single-molecule concentration (3 pM) to stop the reaction, and measured using the technique. The front half population almost entirely disappeared, and populations a, b, and c appeared (in this labeling scheme, the a and b structures are not distinguishable). The method is capable of capturing the c state, an intermediate that was detected 30 s after mixing (B2) and that later almost disappeared (B4). (C) The reaction kinetics profile was constructed by plotting the fraction of the front half population (FH/FH + a + b, the c population is ignored) as a function of the incubation time periods. (C1) Initial reactants concentration of 250 nM and sampling every several dozens of seconds, and (C1) initial reactants concentration of 5, 15, 45, 125, 250 nM and sampling every hundreds of seconds.

required in normal motor operation. To enable the striding process to continue, a 5-fold excess of fuel-2 was added to the mixture, which was then incubated for 1 h and examined using the sm-FRET−ALEX technique. The result clearly shows the appearance of a population with E = 0.15 (Figure 4C, circled with black dashed line), as expected for a scenario in which the two donors were not in close proximity to an acceptor. Here too, the yield of the stepping reaction (85%, RS-2 that transformed to RS-3) was similar to that observed by Omabegho *et al.*[26] (75%).

Monitoring the Assembly Kinetics. To elucidate the mechanisms of the reactions, we measured the kinetic profiles of the walker and front half assembly reactions (Figure 5) and of the leg-lifting reaction upon addition of the fuel strand (Figure 6). In the former, equimolar concentrations of front half and walker (250 nM, Figure 5B1−4 and C1) were cold mixed; mixtures were incubated for various times, diluted to 3 pM to stop the reaction, and examined using the sm-FRET−ALEX technique. The kinetic profile that monitors the presence of the front half comprised a fast phase, followed by a slow phase. In the fast phase, which is faster than (or on the order of) the measurement time resolution (<20 s, the time it takes to mix and dilute the sample), about 50% of the reaction was completed (Figure 5C1). Although the slow phase did increase the reaction yield, the overall yield was not very high. The time resolution of this measurement does not allow a reliable fitting of the fast phase. In principle, it is possible to slow the reaction rate by initiating the reaction with a lower reactants concentration. Unfortunately, lower initial concentration results in lower yields, as can be seen in Figure 5C2, which prevent the acquisition of a detailed kinetic profile. The slow phase was not fitted since its exact origin and corresponding model are unknown (see the Discussion section), and we were careful not to over interpret. An intermediate population, which appears after mixing and disappears with time, was observed (Figure 5 population c). This labeling scheme is not sufficient to conclusively determine the origin of this population. By using a different labeling scheme, we suggest that the c population could be an undesired complex of two tracks and one walker (Supporting Information, Figure S5). Since the walker can bind the nonhairpin T1 faster than the hairpin T2, an intermediate b population, in which the L-O leg is bound to the walker and the L-E leg

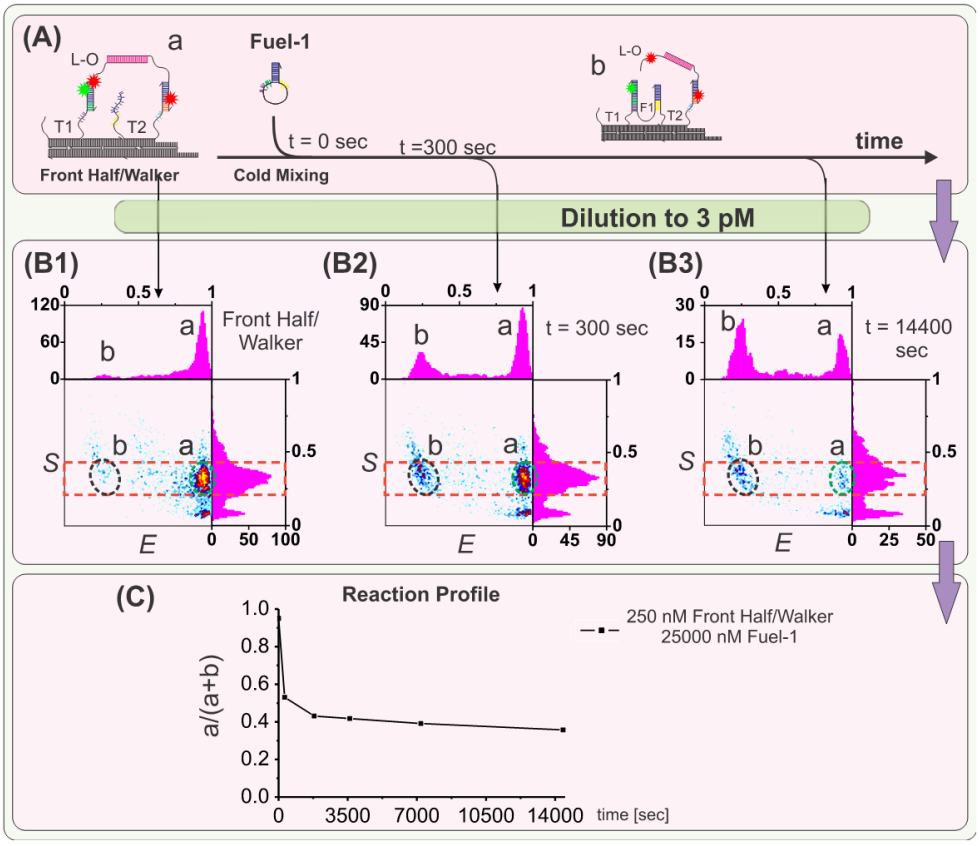

Figure 6. Kinetics of leg lifting upon fuel addition. (A) Fuel-1 is cold mixed with front half/walker (a), binds T2, and forces the lifting of the walker's leg L-O (b). (B1−3) After various incubation periods the mixture is sampled, diluted to single-molecule concentration to stop the reaction, and measured. The population with the lifted leg, which had amounted to just ∼5% before the addition of fuel (B1), grew to ∼45%s after 300 s (B2). The reaction kinetics profile was constructed by plotting the fraction of the a population as a function of the incubation time ($a/(a+b)$) (C). The initial concentration was 250 nM front half/walker complex and 25 000 nM fuel-1.

not, is expected. Figure S5 clearly show the appearance followed by the disappearance of the b intermediate.

Monitoring the Operation Kinetics. A similar picture to that of the assembly reaction kinetic with the fast and slow phases was observed for the leg-lifting reaction. The reaction was initiated by the addition of 100 times excess of fuel-1 to the front half/walker complex (25000 nM and 250 nM, respectively, Figure 6). In the fast phase (<300 s) about 45% of the reaction was completed, and the slow phase contributed about ∼20% to the overall yield. Also here, lowering the initial concentration lowers the yield (data not shown), limiting the ability to slow the reaction. Preliminary results from total internal reflection fluorescence (TIRF) immobilization experiments with time resolution of seconds indicate that the fast phase is in the order of several seconds or faster (Supporting Information, Figure S6).

DISCUSSION

A Successful Demonstration of the Correct Motor Assembly and Operation. From the measurements presented here, we may conclude that the motor was indeed assembled and operates as designed. The *E* and *S* values of the major population are as expected for a correctly assembled and correctly operate motor. We have thus successfully proved the assembly and operation principles of the motor but by a different method than that of Omabegho *et al.*[26] However, the equilibrium single-molecule measurements indicate the presence of side products and incomplete reaction, an observation which is supported by the reaction profiles acquired in the nonequilibrium measurements. We will now discuss these issues.

Reaction Yields. Our measurements show that even simple two ssDNA hybridization reactions do not have very high yields (77−93%, Figure 2), an observation that has previously been reported for other DNA sequences,[23,24] and that we do not understand. Performing these reactions (Figure 2A2−5) by means of annealing did not improve yields (data not shown). The known[27,28] and measured (Figure 5 and 6) binding rates of two ssDNAs and the measured unbinding rates (dsDNA is stable for days at a 1 pM concentration, data not shown) suggest that a careful annealing process should result in reactions with >99% yields. A possible explanation for the lower observed yield could be incomplete labeling or inactive fluorophores. However,

the annealing of the walker's legs L-O and L-E, each time one of them in 25% excess, resulted in almost complete disappearance (<2% remaining) of the non-hybridized population of the minor strand (data not shown), indicating that a lack of active fluorophore is not the only reason for the observed incomplete reaction, although it probably somewhat contribute. For discussion on other possible reasons for the presence of donor- and acceptor-only populations, see the Supporting Information. Further research examining different ssDNA lengths and sequences and different initial concentrations and preparation methods is required to understand the reason for the incomplete hybridization of two complementary ssDNAs. If we wish to achieve highly reliable DNA-based technology, such study is essential. The ability of the ALEX method to separate singly labeled populations from doubly labeled populations makes it the tool of choice to conduct such a study.

Our measurements also showed that formation yields for structures with a higher level of complexity are not very high and that the values are similar to those observed by Omabegho *et al.*[26] (57−95% in this study). This finding is not surprising given the fact that simple hybridization reactions are not complete, as explained, and that the motor design and method of preparation intrinsically lead to the formation of side products (Figure 3C1−2, and Supporting Information, Figures S2, S3 and S5) as explained below. In addition, it is important to remember that the *S* values, from which the reaction yields are calculated, indicate the presence/absence of labeled components and do not provide information on the detailed shape of the complex. Like the gel technique, which indicates mainly size and not structure, it is possible that the formed complex, although having the right size, and in our case, the right stochiometry, is of wrong architecture. *E*, which provides a measure of the donor−acceptor distance, had approximately the expected values in all cases, thus supporting the conclusion that, generally, the designed structures were indeed formed. However, for the more complex structures the presence of additional populations in the *E* or *S* (either distinguished population or histograms' tails, as in Figures 3, 4 and 5) suggest that products with wrong architecture were formed, for example, as demonstrated in the formation of side products (Supporting Information, Figures S2, S3, and S5).

Side Reaction and Products. Several measurements indicate the presence of side products, especially multiple binding of front or back halves and walkers as was seen by Omabegho *et al.*[26] For example, two walkers binding a single front halve is observed in Figure 3 and 4 (circled with green dashed line) (for more measurements indicating these types of side reactions, see Figures S2 and S3 in the Supporting Information). The current motor design allows the binding of two walkers to a single front half and *vice versa*. To remove side products, Omabegho *et al.*[26] used streptavidin-coated magnetic beads and biotinylated ssDNA with a sequence complementary to that of T1 and T2 to immobilize and filter out incorrect structures. Relying on the ability of our method to separate populations based on their stoichiometry, and since it is beyond the purpose of this work to improve the motor, we omitted this step. The measurements presented in Figure 3C1−2, for example, do indeed provide a demonstration of the ability of our method to identify side products and side reactions, an important feature when dealing with complex and often heterogeneous DNA devices. Based on *S* values, the ALEX method enabled the separation of the desired population from one of the side products (C1, circled with green dashed line, but not from the other, C2, circled with red dashed line). The ALEX method thus enabled structure determination (based on *E* values) of the correct population, sorted from the incorrect side product, a feature not provided by bulk-fluorescence techniques.

Reaction Kinetics. After demonstrating correct motor assembly and proper operation, we examined the mechanisms of the assembly and operation reactions by measuring their kinetic profiles. The two reactions examined revealed similar profiles, that is, a fast phase followed by a slow phase. The presence of the fast phase and the initial fast reaction rate is not surprising. The typical rate constant for binding two ssDNAs lacking secondary structures (referring to the binding of the front half to the walker *via* two ssDNAs, Figure 5) is of the order of 10^6−10^5 M^{-1} s^{-1}, corresponding to 4−40 s for half completion of the reaction when the initial concentration is 250 nM,[27,29,28] (as we used here). Thus, the front half T1 and the walker L-O, which lack a secondary structure, are expected to bind roughly as observed in the fast phase. However, the presence of the slow phase and the fact that the fast phase did not bring the reaction to high yields still require explanation. Three possible explanations can be given, none of which seems satisfactory: First, it is possible that the system reaches thermodynamic equilibrium in which the most stable structure (in terms of enthalpy, presumably the front half/walker complex) is dynamically assembled and disassembled. However, this explanation cannot be correct, since in an equilibrium scenario, the ratio of the binding rate to that of the unbinding rate is reflected in the equilibrium constant. Here, the binding rate is very fast, as indicated by the kinetic measurements themselves, but the unbinding rate is very slow, as reflected by the fact that the motors are stable for at least a day even at a concentration of 1 pM (data not shown), yet the yields are as low as 20−80% (corresponding to initial concentrations of 5−250 nM, Figure 5C2). Another possible explanation is that a fraction of the reactants is deformed such that they cannot react properly. However, in such a case,

changing the initial concentration would not influence the reaction yield, in contradiction to our observations (Figure 5C2). Finally, competing reactions, in which a side reaction converts a fraction of the front half or of the walker reactant into a product that is unable to react properly is a reasonable possible explanation, but no such products were identified.

A similar picture, that is, a fast phase followed by a slow phase, was observed for the leg-lifting upon fuel addition (Figure 6 and Supporting Information, Figure S6). Here, too, the presence of the fast phase and the initial high reaction rate are not surprising. The initial step for this reaction is the binding of free ssDNA (of the opened stem loop-2) to a complementary sequence inside the hairpin loop (Figure 1B2), followed by two consecutive branch migration processes, the first to open the hairpin and the second for the opened hairpin to remove L-O from T1 (Figure 1B3−4). The rate-limiting step for opening the hairpin by hybridization to free ssDNA with a binding site inside the hairpin's loop is the binding reaction, with a rate constant of 10^5-10^4 M^{-1} s^{-1}, corresponding to 0.4−4 s for half completion of the reaction when the initial concentration is 25 000 nM,[29] (we mixed 25 000 nM fuel-1 and 250 nM front half/walker complex). Here, too, we found that decreasing the fuel concentration decreased the reaction yield (data not shown). The noncompletion of the reactions measured under nonequilibrium conditions was consistent with the limited yields observed in the equilibrium assembly and operation experiments. Thus, the overall picture that arises is that the assembly and operation reactions take place fairly fast, but with low yields, and that longer incubation times contributed somewhat to the overall yield but do not bring the desired reaction to completion. A careful study, which will examine simpler systems, is required to explain the noncompletion of the reaction and the reaction profiles.

Problems with the Current Strategy of Device Preparation. Several of the DNA devices introduced to date were prepared along lines similar to the motor presented here, that is, building blocks were annealed or cold mixed (or both) for long times (order of many minutes) at high (>100 nM) equimolar concentrations,.[10,11] The rationale underlying this approach is that the designed product is the most stable in means of enthalpy and that the enthalpy will overcome entropy such that eventually under equilibrium conditions, the designed product will dominate. For that reason, the formation reactions were conducted in high concentrations (favoring enthalpy over entropy), and the reactions were allowed to proceed for a long time to promote the formation of the most stable structures. However, this approach is somewhat problematic, as is evident from this study and previous works.[11,18] For example, in cases in which building-block X is designed to bind building-block Y *via* two contact sites, like the front half and walker assembled here or the interaction between tweezers and fuel,[11] the assembly strategy might intrinsically lead to formation of enthalpy-stable side products the following way: instead of X binding Y *via* two contacts, X might bind two Ys which in turn bind an additional X(s) (or vice versa), possibly forming opened or closed chains of various lengths. Since the hybridization sites (the number of the base pairs to interact, thus the strength) are the same as those for the desired product, the side products are not necessarily less stable. Reducing the reactant concentrations, which decreases the binding rate, however, can, in principle, prevent this undesired reaction: X binds Y *via* a single binding site, and before another X or Y binds the complex, X and Y complete the reaction by binding *via* the second binding site, thereby avoiding binding to additional Xs or Ys. In a different system studied by us, which is based on the bipedal nonautonomous motor of Shin *et al.*[10] reducing the reactant concentration increased the yield (data not shown), but, unfortunately, this was not the case in the motor studied here as evident in Figure 5C2.

Suitability and Benefits of the Method. Using a single analytical method, the single-molecule diffusion-based FRET−ALEX technique, we were able to demonstrate the formation and operation of Omabegho's autonomous DNA bipedal motor. The method has several advantages that makes it an excellent analytical tool for developing and studying DNA devices with complexity similar or higher than of the system examined here. In contrast to Omabegho's radioactive gel method, which requires radioactive and psoralen labeling and psoralen-aided state freezing, our method requires only fluorophore labeling. Current labeling procedures have excellent yields and purities (∼70% and >99%, respectively; see Figure S12 in the Supporting Information) and common fluorophores are very photostable, thus, it does not significantly increase the complexity of the data analysis. Furthermore, our method carries the advantages of an *in situ* approach, in which experiments are conducted at device-favorable and native conditions; the only environmental change that the analyte experiences is a harmless dilution. Unlike the gel technique, where the procedure takes about a day, our measurements are fairly simple. The motor is prepared according to the method of Omabegho *et al.*[26] (excluding the psoralen and radioactivity related steps, and the purification), diluted to 3 pM, and measured for 5−15 min (kinetic experiments are run for longer times when required); the data analysis takes another minute, and the interpretation is usually straightforward. The immediate feedback provides several experimental and synthetical benefits. For example, information on the sample stoichiometry enables rapid fine-tuning of the relative concentrations of reactants to achieve equimolar mixtures, giving increased reaction yield, as we did here.

Similarly, other preparation parameters such as ionic strength, annealing temperature profile, and cold mixing incubation time can be rapidly studied and optimized. Furthermore, the fluorescence and *in situ* nature of our method enabled us to carry out nonequilibrium time-dependent experiments from which reaction profiles were acquired. The kinetic profiles contribute to the understanding of the mechanisms that govern the assembly and operation reaction, which can eventually result in improved designs. Finally, short-lived intermediates can be detected, (for example, population b in Supporting Information, Figure S5 and population c in Figure 5) and studied.

CONCLUSIONS

With the aim to harness the advantages of the single-molecule fluorescence approach as an analytical tool to achieve a more rational and intelligent design process for DNA-based devices, we tested whether the method is suitable for monitoring the assembly and operation of one of the most sophisticated and complex DNA devices introduced to date, an autonomous bipedal motor. Although significantly different from the radioactive gel method used originally, our method produced similar conclusions. The motor was generally assembled and operated as designed; the yields of the operation reaction were around 63−85%, and similar side products to those found in the original work were identified. Thus, we have successfully demonstrated the applicability of our method as a useful analytical tool in the field of DNA nanotechnology, in the specific context of the bipedal autonomous motor assembly and operational principles.

Going beyond proof of principle, we applied an extension of the method to measure the time-resolved evolution of the assembly and operation reactions. The fast phases observed in the kinetic measurements were consistent with our expectations, and the incomplete reactions were consistent with our corresponding equilibrium measurements and the findings of Omabegho *et al.*[26] Kinetic measurements of this type are either very difficult or impossible to conduct with the gel technique. Because bulk-fluorescence measurements provide information on the entire ensemble and not specifically on the population of interest, they will fail to estimate the relevant reaction yields. Thus, for reliable and detailed structural dynamic information of complex DNA systems to be acquired, single-molecule fluorescence has to be used. Moreover, the quality and resolution of our results suggest that there is room for systems with increased complexity to be analyzed, and the kinetic measurements demonstrate that the approach is capable of providing *in situ* information with high temporal and spatial resolution on the structural dynamics of complex DNA-based devices and hence of potentially improving preparation and operation strategies.

Our equilibrium and the nonequilibrium data and its analysis suggests that although, in general, the motor assembled and operates as planned, the current preparation and operation strategies are somewhat insufficient if we wish to achieve highly reliable, well constructed, and well operated DNA made nanodevices. Incomplete and undesired assembly reactions (which were not filtered in this work as it was done by Omabegho *et al.*[26]), incomplete operation reactions, and probably harmful interactions between individual motors reduce the overall motor's yield. Alternative designs and assembly and operation strategies have to be developed.

The demonstration of the diffusion-based single-molecule FRET−ALEX technique in this work indicates that other variations of the single-molecule fluorescence approach can be harnessed for different purposes; for example, individual devices can be immobilized and monitored for long times by a total internal reflection fluorescence (TIRF) technique (Supporting Information, Figure S6), enabling measurement of structural dynamics under equilibrium conditions and providing information about the sequence of events. Another possibility is the use of three-color ALEX,[30] which can significantly increase the stoichiometrical and structural information. Data can be analyzed more rigorously to provide information on accurate donor−acceptor distances and distance distributions and hence to facilitate a detailed study of reaction mechanisms; for example, each of the steps taking place from the fuel binding to the leg lifting could be studied separately and in detail.

All in all, this work demonstrates the benefits of utilizing single-molecule fluorescence spectroscopy as a major instrument for the promotion of the DNA nanotechnology field.

METHODS

ssDNA Preparation. HPLC-purified ssDNAs were purchased (IDT Inc., Coralville, LA) and used as is. The dry DNA strands were dissolved in TE buffer (10 mM Tris-Cl and 1 mM EDTA, pH 8) to a final concentration of 1 mM and stored at −20 °C. To prevent degeneration of the adenine base, a basic environment (pH > 8) was ensured.

Fluorophores. ATTO 550 and the ATTO 647N are ideal fluorophores for single-molecule diffusion-based experiments. The fluorophores are photostable in a DNA environment (low bleaching and blinking levels), bright (high extinction coefficients and quantum yields), and exhibit absorption maxima fit to common lasers (532 and 640 nm excitation lasers), minimum direct excitation (the donor laser does not excite the acceptor dye), and minimum donor-leakage (donor emission leaks to the acceptor channel). The typical resultant bursts are consistent with 200−2000 photons.

ssDNA Labeling. HPLC-purified ssDNAs were purchased with a C6 dT internal amino modifier (iAmMC6T) in the designed

position. ATTO 550 or ATTO 647N (donor and acceptor, respectively, ATTO-TECH GmbH, Siegen, Germany) were labeled and HPLC purified (reverse-phase C18, Amersham Bioscience, Uppsala, Sweden) by using improved procedures (see Supporting Information). The typical labeling yield was ~70% and purity was >99%, as checked by reintroduction to the HPLC.

Buffers. The buffer solution for maintaining in stock the samples for annealing and for cold mixing was 10.5 mM Mg-TAE (40 mM Tris-base, 2 mM EDTA.$Na_2 \cdot 2H_2O$ and 20 mM acetic-acid, pH 8), as in Omabegho *et al.*[26] All ssDNAs were kept at a concentration of 10 μM, as verified by the absorption in 260 nm by using a UV−vis spectrophotometer (Helios Omega UV−visible).

Annealing. The annealing procedure was conducted at an ssDNAs concentration of 500 nM with a PCR machine [90 °C (5 min), 65 °C (20 min), 45 °C (20 min), 37 °C (20 min), room temperature (20 min), altogether 1.5 h], as in Omabegho *et al.*[26] (who used a heating block). The sample volume was 10−30 μL, such that 5−15 picomole of each strand were required.

Cold Mixing. Typically 1−10 picomoles of each strand were mixed for 1 h at room temperature and at 100−500 nM ssDNA concentrations (as detailed in the text), in a volume of 10−20 μL.

Assembly of the Front Half, Back Half, and Walker. The front half contains S1−S7 (20−42 bases long) and T1-T2 (67 and 83 bases long) strands. Ten picomole of each strand was mixed together to make a 20 μL solution (500 nM of each strand), and annealed. The back half contained S8−S14 (20−42 bases long), and T3-T4 (83 bases), and the walker contained L-O and L-E (54 bases) that were similarly and separately prepared.

Assembly of the Complete Track. A solution of 5 μL of the front half (500 nM) was cold mixed for 1 h with 5 μL of the back half (500 nM), resulting in a 10 μL of 250 nM complete track.

Assembly of the Front Half/Walker Complex. A solution of 5 μL of walker (500 nM) was cold mixed for 1 h with 5 μL of front half (500 nM), giving 10 μL of 250 nM front half/walker complex.

Assembly of the Complete Motor. To assemble the complete motor, 5 μL of front half/walker (250 nM) were cold mixed for 1 h with 2.5 μL of back half (500 nM), giving 7.5 μL of 167 nM complete motor and RS-1.

Operation of the Complete Motor. Before adding the fuel strands to the solution of the motor, each fuel strand was heated separately (90 °C for 5 min and then cooled immediately to room temperature) to ensure correct folding (properly closed hairpin). Transition from RS-1 to RS-2 was achieved by cold mixing of the complete track at RS-1 with a 5-fold excess of fuel-1 (to give 6.5 μL of 148 nM RS-1 and 740 nM fuel-1) for 1 h. Similarly, the transition from RS-2 to RS-3 was achieved by cold mixing the RS-2 with a 5-fold excess of fuel-2 (to give 9 μL of 99 nM RS-1 and 495 nM fuel-2) for 1 h.

Measurements. All measurements were carried out on diluted samples (20 μL of 3 pM) that were placed on a coverslip and sealed with Teflon and an upper coverslip. The bottom coverslip was KOH-treated to prevent the samples, especially the larger complexes, from sticking to the surface (as happens in the presence of Mg^{2+}), sonicated for 15 min, washed with distilled water and dried in air. The measurement buffer comprised 10 mM Tris-Base pH 8, 1 mM EDTA, 10 μg/mL bovine serum albumin (BSA, Sigma-Aldrich, Co) to reduce sample sticking, 10.5 mM Mg acetate, and 1 mM Trolox to reduce photobleaching and photoblinking,[31] (Sigma-Aldrich, Co). With the exception of the kinetic experiments, data were collected over 5−15 min.

Calculating Reaction Yields. Reaction yields for the motor assembly in Figure 2, were calculated by dividing the number of bursts (events) of the donor−acceptor population ($0.15 < S < 0.85$ to exclude donor and acceptor only population) into the overall number of bursts. The yield of the front half/walker complex formation reaction in Figure 3 was calculated by dividing the number of bursts inside the black dashed line into the overall number of bursts. The Reaction yields for the motor operation in Figure 4 were calculated by dividing the number of bursts of the final state (RS-2 and RS-3, circled with black dashed line) into that of the initial plus the final states (RS-1 + RS-2 and RS-2 + RS-3, circled with red and black dashed lines, respectively).

Front Half/Walker Binding Kinetics. Preannealed walker (500 nM) and preannealed front half (500 nM) were cold mixed in various equimolar concentrations (250, 125, 45, 15, and 5 nM). After various time periods, 1 μL of the solution was sampled, diluted to 3 pM to stop the reaction, and measured.

Front Half/Walker Leg-Lifting Kinetics. The front half/walker complex (250 nM) was cold mixed with a 100-fold excess of fuel-1 to give 10 μL. After various time periods, 1-μL aliquots of the solution were sampled, diluted to 3 pM, and measured.

Theory. Since in ALEX experiments two lasers alternatively excite the donor and the acceptor dyes, the calculation of E is somewhat different from that in a conventional single laser experiment:

$$E = \frac{A_{D_{EX}}}{D_{D_{EX}} + A_{D_{EX}}} \quad (1)$$

where $D_{D_{EX}}$ is the number of photons recorded in the donor channel and $A_{D_{EX}}$ is the number of photons recorded in the acceptor channel during times in which the donor laser is on (donor laser "on time"). As is commonly defined in ALEX experiments,[25] stoichiometry or brightness ratio, S, is calculated by dividing the sum of the photons recorded in the donor and the acceptor channels during donor laser on-time by the sum of the photons recorded in both channels during donor laser and acceptor laser on-times:

$$S = \frac{D_{EX}}{D_{EX} + A_{EX}} \quad (2)$$

where D_{EX} and A_{EX} are the sums of photons recorded in the donor and the acceptor channels during donor laser and acceptor laser on-times, respectively.

Data Analysis and Presentation. The data analysis was performed with the in-house written Labview (National Instruments 7.1) software as described above.[24] The beginnings and ends of bursts were determined by using the all-photons-burst-search (APBS)[24] (parameters: L = 200, M = 10, and T = 200 μs). According to the algorithm, a photon belongs to a burst if each of at least L successive photons has at least M neighboring photons within a time window of length T centered on the photon's own arrival time. For each burst, E and S were calculated according to eq 1 and eq 2, respectively, binned (0.01 bin size), and plotted on one-dimensional E and S and histograms on a two-dimensional E/S histogram.

Optical Setup. The sm-FRET−ALEX experiments were carried out on an in-house built optical setup as described in a previous work,[24] (for more details, see Supporting Information). The setup was stable over the entire period, and except for minor tunings of the excitation power, no adjustments were required.

Conflict of Interest: The authors declare no competing financial interest.

Acknowledgment. The authors thank Nadrian Seeman and Tosan Omabegho, for many fruitful and inspired discussions, their suggestions and comments were of a great help. Tosan Omabegho also read the manuscript; we thank him for his comments. We thank Tatyana Gavrinyov for the help provided with the high-performance liquid chromatography.

Supporting Information Available: Detailed description of the sm-FRET−ALEX technique, optical setup, and scope; list of differences between this work and Omabegho *et al*;[26] additional single molecule data indicating side reaction, front half/walker formation, intermediates, and fast leg lifting reaction using TIRF; detailed description of sample perpetration, including DNA labeling and purification procedures, motor structure, and DNA sequences. This material is available free of charge *via* the Internet at http://pubs.acs.org.

REFERENCES AND NOTES

1. Sacca, B.; Niemeyer, C. M. DNA Origami: The Art of Folding DNA. *Angew. Chem., Int. Ed. Engl.* **2012**, *51*, 58–66.
2. Simmel, F. C. Processive Motion of Bipedal DNA Walkers. *ChemPhysChem* **2009**, *10*, 2593–2597.

3. von Delius, M.; Leigh, D. A. Walking Molecules. *Chem. Soc. Rev.* **2011**, *40*, 3656–3676.
4. Lund, K.; Manzo, A. J.; Dabby, N.; Michelotti, N.; Johnson-Buck, A.; Nangreave, J.; Taylor, S.; Pei, R. J.; Stojanovic, M. N.; Walter, N. G.; *et al.* Molecular Robots Guided by Prescriptive Landscapes. *Nature* **2010**, *465*, 206–210.
5. Qian, L. L.; Winfree, E. Scaling up Digital Circuit Computation with DNA Strand Displacement Cascades. *Science* **2011**, *332*, 1196–1201.
6. Gu, H. Z.; Chao, J.; Xiao, S. J.; Seeman, N. C. A Proximity-Based Programmable DNA Nanoscale Assembly Line. *Nature* **2010**, *465*, 202–205.
7. Douglas, S. M.; Bachelet, I.; Church, G. M. A Logic-Gated Nanorobot for Targeted Transport of Molecular Payloads. *Science* **2012**, *335*, 831–834.
8. Wickham, S. F.; Bath, J.; Katsuda, Y.; Endo, M.; Hidaka, K.; Sugiyama, H.; Turberfield, A. J. A DNA-Based Molecular Motor That Can Navigate a Network of Tracks. *Nat. Nanotechnol.* **2012**, *7*, 169–173.
9. Wickham, S. F.; Endo, M.; Katsuda, Y.; Hidaka, K.; Bath, J.; Sugiyama, H.; Turberfield, A. J. Direct Observation of Stepwise Movement of a Synthetic Molecular Transporter. *Nat. Nanotechnol.* **2011**, *6*, 166–169.
10. Shin, J. S.; Pierce, N. A. A Synthetic DNA Walker for Molecular Transport. *J. Am. Chem. Soc.* **2004**, *126*, 10834–10835.
11. Yurke, B.; Turberfield, A. J.; Mills, A. P.; Simmel, F. C.; Neumann, J. L. A DNA-Fuelled Molecular Machine Made of DNA. *Nature* **2000**, *406*, 605–608.
12. Wozniak, A. K.; Schroder, G. F.; Grubmuller, H.; Seidel, C. A.; Oesterhelt, F. Single-Molecule FRET Measures Bends and Kinks in DNA. *Proc. Natl. Acad. Sci. U.S.A* **2008**, *105*, 18337–18342.
13. Zhao, R.; Rueda, D. Rna Folding Dynamics by Single-Molecule Fluorescence Resonance Energy Transfer. *Methods* **2009**, *49*, 112–117.
14. Pirchi, M.; Ziv, G.; Riven, I.; Cohen, S. S.; Zohar, N.; Barak, Y.; Haran, G. Single-Molecule Fluorescence Spectroscopy Maps the Folding Landscape of a Large Protein. *Nat. Commun.* **2011**, *2*), 1504–1505.
15. Roy, R.; Kozlov, A. G.; Lohman, T. M.; Ha, T. Dynamic Structural Rearrangements between DNA Binding Modes of *E. coli* SSB Protein. *J. Mol. Biol.* **2007**, *369*, 1244–1257.
16. Gansen, A.; Valeri, A.; Hauger, F.; Felekyan, S.; Kalinin, S.; Toth, K.; Langowski, J.; Seidel, C. A. Nucleosome Disassembly Intermediates Characterized by Single-Molecule FRE. *Proc. Natl. Acad. Sci. U.S.A* **2009**, *106*, 15308–15313.
17. Rajendran, A.; Endo, M.; Sugiyama, H. Single-Molecule Analysis Using DNA Origami. *Angew. Chem., Int. Ed.* **2012**, *51*, 874–890.
18. Muller, B. K.; Reuter, A.; Simmel, F. C.; Lamb, D. C. Single-Pair FRET Characterization of DNA Tweezers. *Nano Lett.* **2006**, *6*, 2814–2820.
19. Goodman, R. P.; Heilemann, M.; Doose, S.; Erben, C. M.; Kapanidis, A. N.; Turberfield, A. J. Reconfigurable, Braced, Three-Dimensional DNA Nanostructures. *Nat. Nanotechnol.* **2008**, *3*, 93–96.
20. Steinhauer, C.; Jungmann, R.; Sobey, T. L.; Simmel, F. C.; Tinnefeld, P. DNA Origami as a Nanoscopic Ruler for Super-Resolution Microscopy. *Angew. Chem., Int. Ed.* **2009**, *48*, 8870–8873.
21. Roy, R.; Hohng, S.; Ha, T. A Practical Guide to Single-Molecule FRET. *Nat. Methods* **2008**, *5*, 507–516.
22. Tomov, T. E.; Tsukanov, R.; Masoud, R.; Liber, M.; Plavner, N.; Nir, E. Disentangling Subpopulations in Single-Molecule FRET and ALEX Experiments with Photon Distribution Analysis. *Biophys. J.* **2012**, *102*, 1163–1173.
23. Kapanidis, A. N.; Laurence, T. A.; Lee, N. K.; Margeat, E.; Kong, X.; Weiss, S. Alternating-Laser Excitation of Single Molecules. *Acc. Chem. Res.* **2005**, *38*, 523–533.
24. Nir, E.; Michalet, X.; Hamadani, K. M.; Laurence, T. A.; Neuhauser, D.; Kovchegov, Y.; Weiss, S. Shot-Noise Limited Single-Molecule FRET Histograms: Comparison between Theory and Experiments. *J. Phys. Chem. B* **2006**, *110*, 22103–22124.
25. Kapanidis, A. N.; Lee, N. K.; Laurence, T. A.; Doose, S.; Margeat, E.; Weiss, S. Fluorescence-Aided Molecule Sorting: Analysis of Structure and Interactions by Alternating-Laser Excitation of Single Molecules. *Proc. Natl. Acad. Sci. U.S.A* **2004**, *101*, 8936–8941.
26. Omabegho, T.; Sha, R.; Seeman, N. C. A Bipedal DNA Brownian Motor with Coordinated Legs. *Science* **2009**, *324*, 67–71.
27. Morrison, L. E.; Stols, L. M. Sensitive Fluorescence-Based Thermodynamic and Kinetic Measurements of DNA Hybridization in Solution. *Biochemistry* **1993**, *32*, 3095–3104.
28. Turberfield, A. J.; Mitchell, J. C.; Yurke, B.; Mills, A. P., Jr.; Blakey, M. I.; Simmel, F. C. DNA Fuel for Free-Running Nanomachines. *Phys. Rev. Lett.* **2003**, *90*), 1–4.
29. Green, S. J.; Lubrich, D.; Turberfield, A. J. DNA Hairpins: Fuel for Autonomous DNA Devices. *Biophys. J.* **2006**, *91*, 2966–2975.
30. Hohng, S.; Joo, C.; Ha, T. Single-Molecule Three-Color FRET. *Biophys. J.* **2004**, *87*, 1328–1337.
31. Cordes, T.; Vogelsang, J.; Tinnefeld, P. On the Mechanism of Trolox as Antiblinking and Antibleaching Reagent. *J. Am. Chem. Soc.* **2009**, *131*, 5018–5019.